Author/s:
Chew, GL;Huang, D;Lin, SJ;Huo, C;Blick, T;Henderson, MA;Hill, P;Cawson, J;Morrison, WA;Campbell, IG;Hopper, JL;Southey, MC;Haviv, I;Thompson, EW

Title:
High and low mammographic density human breast tissues maintain histological differential in murine tissue engineering chambers

Date:
2012-08-01

Citation:
Chew, G. L., Huang, D., Lin, S. J., Huo, C., Blick, T., Henderson, M. A., Hill, P., Cawson, J., Morrison, W. A., Campbell, I. G., Hopper, J. L., Southey, M. C., Haviv, I. & Thompson, E. W. (2012). High and low mammographic density human breast tissues maintain histological differential in murine tissue engineering chambers. Breast Cancer Research and Treatment, 135 (1), pp.177-187. https://doi.org/10.1007/s10549-012-2128-z.

Persistent Link:
https://hdl.handle.net/11343/220063

Title Page

High and Low Mammographic Density Human Breast Tissues Maintain Histological Differential in Murine Tissue Engineering Chambers

[1]GL Chew, [2]D Huang, [3,4]SJ Lin, [1]C Huo, [2]T Blick, [1,3]MA Henderson, [4,5]P Hill, [6]J Cawson, [1,7]WA Morrison, [3]I Campbell, [8]J Hopper, [4]M Southey, [9]I Haviv, [1,2]EW Thompson

[1]University of Melbourne Department of Surgery, St Vincent's Hospital, [2]St Vincent's Institute, [3]Peter MacCallum Cancer Center, [4]Department of Pathology, University of Melbourne, [5]St Vincent's Pathology, Melbourne, [6]St Vincent's BreastScreen, St Vincent's Hospital Campus, University of Melbourne, [7]O'Brien Institute of Microsurgery, [8]School of Population Health, University of Melbourne, Australia and [9]Faculty of Medicine, Bar Ilan University, Zfat, Israel.

Corresponding author: GL Chew; e-mail: grace.chew@svhm.org.au; telephone: +613 9288 2211; fax: +613 9288 4737

Abstract

Introduction: Mammographic density (MD) is the area of breast tissue that appears radiologically white on mammography. Although high MD is a strong risk factor for breast cancer, independent of BRCA1/2 mutation status, the molecular basis of high MD and its associated breast cancer risk is poorly understood. MD studies will benefit from an animal model, where hormonal, gene and drug perturbations on MD can be measured in a preclinical context.

Methods: High and low MD tissues were selectively sampled by stereotactic biopsy from operative specimens of high-risk women undergoing prophylactic mastectomy. The high and low MD tissues were transferred into separate vascularised biochambers in the groins of SCID mice. Chamber material was harvested at six weeks for histological analyses, and immunohistochemistry for cytokeratins,

vimentin and a human-specific mitochondrial antigen. Within-individual analysis was performed in replicate mice, eliminating confounding by age, body mass index and process-related factors, and comparisons were made to the parental human tissue. Maintenance of differential MD post-propagation was assessed radiographically.

Results: Immunohistochemical staining confirmed the preservation of human glandular and stromal components in the murine biochambers, with maintenance of radiographic MD differential. Propagated high MD regions had higher stromal ($p=0.0002$) and lower adipose ($p=0.0006$) composition, reflecting the findings in the original human breast tissue, although glands appeared small and non-complex in both groups. No significant differences were observed in glandular area ($p=0.4$) or count ($p=0.4$) between high and low MD biochamber tissues.

Conclusion: Human mammary glandular and stromal tissues were viably maintained in murine biochambers, with preservation of differential radiographic density and histological features. Our study provides a murine model for future studies into the biomolecular basis of MD as a risk factor for breast cancer.

Keywords: Mammographic density; murine; bioengineering chambers; breast density; stroma

Introduction

Mammographic density (MD) refers to the area of radiologically white tissue on a mammogram [1], and percent MD (PMD) is the proportion of MD area on a mammogram. High PMD carries significant clinical importance, as it is the strongest risk factor for breast cancer, after age and BRCA1/2 mutation, when adjusted for BMI [2,3]. The breast cancer risk associated with the highest PMD category is four to six times greater than the lowest category [4-8]. Reduction in PMD was also a significant indicator of reduction in breast cancer risk in the IBIS-1 prevention trial with Tamoxifen [9]. This provides an impetus for the evaluation of MD as a biomarker for breast cancer risk, and suggests a role for MD in predicting response to Tamoxifen [10].

The molecular basis of high MD and its associated breast cancer risk is poorly understood. PMD appears to be most influenced by the relative proportions of fat and stroma, where stromal, epithelial cells and collagen may contribute to the radiographic density in mammograms [11,12]. We previously examined high and low MD material sampled by stereotactic biopsy from within the same breast, finding that high MD areas had increased dense connective tissue and reduced fat, as well as a trend towards smaller epithelial glands, with increased perimeter [13].

Currently, there are few suitable animal models in which to study MD. While radiological examination of mouse mammary fat pads (MFPs) *in vivo* and *ex vivo* has been described [14], quantification of MFP radiographic density is yet to be established. Here we describe an *in vivo* biochamber xenograft system in xenograft SCID mice as a model of human MD. Maintenance of MD characteristics was assessed in stromal, epithelial and adipose elements of human mammary tissue propagated in the pseudo-orthotopic mouse mammary environment using histologic and radiographic analyses [15,16]. The observed preservation of human MD features in the biochamber enables future molecular investigations on the biology of MD.

Method

Accrual of high- and low-MD regions of the same breast: The study was conducted in accordance with the Australian National Statement on Ethical Conduct in Human Research (2007), with approval from Peter MacCallum Human Research Ethics Committee (#08/21) and St Vincent's Hospital Animal Ethics Committee (049/09). Fifteen high-risk women undergoing prophylactic mastectomy at St. Vincent's Hospital were consented through the Victorian Cancer Biobank (VCB 10010).

The mammograms of each participant were examined by a breast radiologist and their Birads category noted. Targeted sampling of high and low MD regions of the mastectomy specimen was performed with SenoRx 10 Gauge stereotactic vacuum-assisted biopsies (Supplementary Fig. 1), as previously described [13]. The regions biopsied were away from any potential malignancies or suspicious microcalcifications. Keeping the tissues viable and sterile, these high and low MD biopsies were partitioned for murine biochamber propagation, histological analysis (formalin-fixed, paraffin-embedded and OCT), and for future analysis (snap frozen in liquid nitrogen).

Bio-engineering chambers in SCID mice: To test the stability of human breast MD within mouse xenograft chambers, high and low MD tissue sampled from within the same fresh mastectomy specimen was minced, mixed 1:1 with Matrigel (BD Biosciences, Bedford, MA) and supplemented with FGF-2 (1 μg/ml, Sigma-Aldrich, Sydney, Australia), then implanted into separate silicone biochambers in the right and left groins respectively of multiple SCID mice (n=3-7), and sustained by the mouse epigastric pedicles, as previously described (Supplementary Fig. 1) [15,16]. Material from the murine biochambers was harvested at six weeks. At harvest, the resultant tissue from each chamber was examined radiographically and histologically.

Histological analysis: Paraffin-embedded tissue sections (4 μm) were stained with haematoxylin and eosin (H+E). The slides were assessed with digital photomicroscopy. Images were exported into image analysis software JMicroVision v1.2.7, and the image of the whole section used to quantify percentage and absolute areas of epithelial, adipose and stromal tissue components. The perimeter of the biochamber or mastectomy biopsy material was demarcated to determine its total area, then a thresholding mask applied for each of the stromal and glandular components before their respective

areas were determined [13,17]. The adipose area was calculated by subtracting stromal and glandular areas from the total area.

Immunohistochemistry: Human cells were distinguished from murine cells by anti-human mitochondrial antibody (h-mito Ab) (Thermo Scientific Mitochondria Ab-2, Clone MTC02, Cat. #MS-1372-P1)) and Vimentin (V9) (DakoCytomation, Clone V9, Code M0725) staining. These were validated in control experiments containing mouse tissue only as the negative control, and human tissue only as a positive control. Pan-cytokeratin (CK) (DakoCytomation, Clone MNF116, Code M0821) staining was performed to identify epithelial cells. To assess the distribution of collagen in relation to glandular epithelium, Masson's Trichrome Blue (MTB) staining was performed. Cellular proliferation in the biochamber and mastectomy tissues was assessed with Ki67 antibody (DakoCytomation, Clone MIB-1, Code M7240) staining. Oestrogen receptor (ER) status was determined with ER antibody (Ventana, Clone SP1, Cat. #790-2223).

Radiographic analysis: Maintenance of high and low MD phenotype after propagation in the biochambers was examined using Faxitron imaging (Faxitron X-ray Corp., Model MX-20; 35 keV, 10 seconds) under precalibrated conditions such that MD could be assessed in a linear range. A calibration strip comprising exponentially stepped transparency sheets placed on each film to enable standardization of x-ray densitometry in relative densitometry units. Matched pairs of propagated high and low MD biochamber cores, cut to the same thickness (2 mm), were imaged. The faxitron image was digitized and analyzed using a densitometer. Image analysis software (JMicroVision v1.2.7) was used to determine the mode of signal intensity for each core, compared to the signal intensity of the calibration strip.

Statistical analysis: High and low MD tissue accrued from the same breast was implanted in matched biochambers of each mouse, thus we performed 'within-individual' analysis to eliminate confounding by external factors. Normality was assessed using the D'Agostino and Pearson Omnibus normality test prior to determining statistical significance. To compare the percentage tissue composition, glandular counts and relative densitometry between high and low MD biochamber tissues, paired t-tests were used for parametric data (GraphPad Prism). The percentage tissue composition of the murine

biochamber and the original mastectomy biopsy tissues were compared using unpaired t-tests. The composition of biochamber tissue elements of high MD tissue originating from women with a BRCA mutation was compared to non-carriers, using unpaired t-tests. The p-value of significance for rejecting a null hypothesis was 0.05.

Results

Study sample

The study sample comprised of paired high and low MD biopsies from fifteen women who underwent prophylactic mastectomy, selected from the Breast Multidisciplinary Meeting. The demographic characteristics of the women are shown in Tables 1 and 2.

Preservation of Histological Differential

On H+E staining of the high and low biochamber tissue sections, mammary epithelial glandular structures formed by epithelial cells with ductal and lobular architecture were visible within the stromal compartment (Fig. 1). Morphologically, the glandular structures in both the high and low MD tissue from the biochambers (Figs. 1 (a) and (b)) appeared smaller and less complex than the original mastectomy tissue (Figs. 1 (c) and (d)). This contrasted with the parental material, where such smaller and less complex glands were seen preferentially in high MD tissues [13].

The organisation of the stromal and adipose elements was also preserved, reflecting similar histological findings in the original biopsies of high and low MD human tissues (Fig. 1). The stromal tissues contained viable stromal cells, and collagen that stained with MTB (Fig 2). MTB staining revealed increased amount of collagen in high compared to low MD chamber tissues, although in both cases the collagen had a similar distribution adjacent to glandular structures in a circumferential manner (Fig. 2).

Preservation of glandular and stromal structures of human origin

Pan-cytokeratin and vimentin staining of the biochamber tissues revealed preserved epithelial glandular and stromal structures respectively, consistent with findings in the original human breast tissue (Figs. 1, 3 (a) and (b)) [13]. Vimentin and h-mito Ab staining is human-specific [16]. The appearance of brown-speckled h-mito Ab staining within the cytoplasm of mammary epithelial and stromal cells, and vimentin in stromal cells, of high and low MD biochambers (Fig. 3(c) and (d)), confirms the persistence of human mammary and stromal structures after propagation in the murine biochambers. These human glandular structures demonstrated an orderly ductal and lobular architecture within human stromal tissue.

In one instance, a few smaller rudimentary mouse mammary ducts were noted in adipose tissue near the artery and vein of the murine epigastric pedicle, similar to those seen in previous studies [15]. These did not take up the h-mito Ab stain, confirming their murine origin (Supplementary Fig. 4 (a)). The majority of adipose cells did not stain with h-mito Ab, but stained with murine-active vimentin antibody, indicating murine origin (Supplementary Fig. 4 (b)).

The high and low MD biochamber glandular tissue had similar ER expression compared to the original human mastectomy biopsies (Figs. 4(a) and (b)), with no difference between ER staining of high and low MD biochamber tissues (Figs. 4(c) and (d)). ER staining was most prominent in luminal glandular epithelial nuclei of both mastectomy biopsy and biochamber tissues.

Proliferation of glandular and stromal cells within biochambers

Ki67 staining indicated cellular proliferation within both glandular and stromal cells in high and low MD biochamber tissues (Figs. 5(c) and (d)). There was no difference between Ki67 rates of high and low MD biochamber tissues (Fig 5). However, the biochamber tissues had increased glandular Ki67 expression compared to the original human mastectomy biopsies (Figs 5(a) and (b)).

Quantitative analysis of biochamber tissue components

Analysis of matched data for the percentage composition of stroma, fat and glandular tissue in the biochamber and mastectomy tissues each revealed a normal distribution. Paired analysis of tissue component areas in the high and low MD biochamber material with t-tests revealed a significant difference in the percentage area of stroma ($p=0.0002$) and fat ($p=0.0006$), with increased stromal and decreased adipose content in high MD chamber tissues (Fig. 6(a)). No difference was observed in the gland percentage area between high and low MD chamber tissues ($p=0.4$) (Fig. 6(a)). When comparing the percentage area composition of the high and low MD biochamber tissue components to the original high and low MD human breast biopsies, there was a similar histological composition (Fig. 6(b)); the high MD human breast biopsies likewise had increased stromal ($p=0.0007$), decreased fat ($p=0.002$) and no difference in glandular areas ($p=0.7$). Quantification of the glands in high and low MD biochamber tissues (Supplementary Fig. 2) did not reveal a significant difference in gland numbers ($p=0.4$).

The stromal, adipose and glandular areas of tissue harvested from high MD biochambers that originated from women who carried a BRCA1/2 mutation were compared to the high MD biochamber tissues of non-carriers. There was no difference in the stroma ($p=0.6$), adipose ($p=0.7$) or gland areas ($p=0.3$) between high MD biochamber tissues of these two groups of women (Fig. 7).

Radiographic analyses of biochamber tissue post-propagation

Faxitron imaging of propagated high and low MD material confirmed that the high MD tissue appeared white on a dark background, and low MD tissue appeared grey on a dark background (Supplementary Fig. 3). Qualitatively, the high MD biochamber tissue appeared lighter than the propagated low MD tissue, against the dark background. Quantitative analysis with densitometry and computerized image analysis of signal intensity of high and low MD biochamber tissues from within the same patients (Fig. 8) confirmed that propagated high MD cores had higher relative densitometry compared to low MD cores ($p=0.0004$).

Discussion

Conservation of MD histological phenotype and radiographic density of biochamber tissues

Using stereotactic methods, we precisely sampled high and low MD regions within the same breast, and described their associated histological features in a previous study [13]. Here we assessed the maintenance of differential MD histology after propagation of high and low MD human tissue in murine biochambers, with correlation to known histological findings in the original breast tissue [13]. Comparing the high MD biochamber tissue histology to that of the original mastectomy biopsies, the high MD mastectomy biopsies similarly had increased stromal and decreased fat areas, suggesting that the MD histological phenotype is conserved in this model. Immunohistochemistry assessment (ER, vimentin, pan-cytokeratin) of high and low MD biochamber tissue also reflected similar findings to that in original mastectomy tissue biopsies.

To quantify the degree of MD in the sub-organ level of human breast core biopsies, we previously described a method of faxitron analysis (using percent area of high and low MD areas within the biopsy [13]). We were able to adapt this to the murine biochambers, allowing reproducible and standardized comparisons of the radiographic density of high and low MD biochamber tissues across multiple experiments. The high MD human breast tissue propagated in murine biochambers for six weeks maintained an increased radiographic density, and the degree of this increased density was measurable as multiples of a standardized unit (relative densitometry unit).

Preservation of human mammary structures and stromal microenvironment

We confirmed the maintenance of human mammary ducts and lobules adjacent to human stromal cells, stained with h-mito Ab and Vimentin, within the high and low MD biochamber environment. The occasional mouse mammary gland was seen to invade adipose tissue near the neurovascular pedicle and persist as rudimentary glands.

Nuclear staining with Ki67 antibody demonstrated that proliferation of stromal and human mammary epithelial cells occurred in the biochambers over six weeks. This is important given the role of epithelial-stromal interactions, where signals between epithelial cells, fibroblasts and extracellular-

matrix in the breast microenvironment can give rise to enhanced cellular proliferation and invasion, leading to development and progression of breast cancer [18-22]. The exact contribution and interplay of the cells and processes that result in the increased malignancy risk associated with MD is unclear, thus a model of MD that maintains these human compartments in a dynamic manner is crucial.

In studies of human breast epithelial cell lines grafted into mouse models, the mice were often supplemented with subcutaneous steroid hormone pellets, because of the lower levels of serum oestradiol in mice compared to humans. During our initial biochamber experiments, we observed that the de novo murine serum oestradiol level was sufficient to maintain glandular structures of human origin within the biochambers for six weeks, without addition of hormone pellets. We also observed similar levels of ER staining in the glandular epithelium of parental mastectomy and biochamber tissues, suggesting preservation of the ER phenotype. Moreover, the matched-pairs study design allows for elimination of any potential confounding from lower murine serum oestradiol systemically.

Small and less complex glandular structures were seen in both low and high MD biochambers compared to the parental mastectomy biopsies. A potential explanation is that during the biochamber propagation process, only the stem-like mammary cell population survived to form small glands [23]. Ki67 expression was greater in biochamber tissues compared to the original mastectomy tissue, suggesting that high and low MD glandular tissues may respond to stimuli within the biochamber microenvironment.

Increased stromal and collagen content

Paired analysis confirmed a greater proportion of dense stromal tissue and collagen in high compared to low MD chamber tissue. This increased stromal content has been observed in several studies examining the histology of high MD samples in women [13,24], and provides further evidence for the validity of the biochamber model. In a mouse model examining the increased breast cancer risk during postpartum involution, Lyons et al [25] demonstrated that radial alignment of collagen fibres and increased COX-2 expression may drive the formation of ductal carcinoma in situ. Provenzano et al [20] have proposed that increased matrix stiffness could partly explain the increased cancer risk in high

MD. Transgenic mice engineered with collagen that resisted normal enzymatic clearance led to premalignant changes, and when combined with a mammary oncogene, caused increased tumour formation, with more invasive and metastatic potential [26]. The biochamber model provides an opportunity to test the role of collagen and extracellular matrix in subsequent studies.

Few existing models of MD

Despite large epidemiological studies demonstrating that high MD is a significant risk factor for breast cancer [6,5,7,8,3], the mechanisms of how high MD promotes breast carcinogenesis remains unclear. A robust animal model for studying MD *in vivo* may ultimately clarify this. Harari et al investigated the radiographic density and histology of murine MFPs deficient in epithelial structure, and containing hyperplastic or malignant epithelium [14]. Digitized images of MFP whole mounts, with epithelial mass and breast density measurement using computer-aided thresholding has been described [27].

As such, few animal models of *murine* mammary density exist to date, due to various challenges, including the lack of standardized measurement of mammary gland radiographic density, and difficulty in maintaining MD over a sufficient duration to enable tumorigenesis. Moreover, the composition of the rodent mammary gland is quite different from the human, thus may not accurately reflect the alterations in human MD and its implications. The murine gland contains small epithelial structures within a larger amount of adipose tissue, and less stromal tissue, compared to the human mammary gland.

Strengths and limitations of the model

Currently, there is no orthotopic xenograft model that can recapitulate *human MD,* with the potential for manipulation of its microenvironment to investigate MD and its role in oncogenesis. Prior to our study, quantitative histological and radiographic analyses of high and low MD *human mammary* tissues in an animal model have not been reported. This murine model is the first to demonstrate maintenance of human mammary glandular structures and stromal tissue within high and low MD chamber tissues for the purpose of modeling MD and its associated risk. Ki67 staining of the biochamber tissues

indicates that cellular proliferation can occur in human glandular and stromal structures during the six weeks. If the high and low MD tissue of human origin responds in a dynamic manner to changes in the biochamber microenvironment, it may be amenable to interventional studies of endocrine, drug and gene manipulation. The driving molecular variables around lifestyle milestones in a woman that can modulate MD, such as pregnancy and postpartum mammary involution, are under investigation in the biochamber model.

One potential issue is that the high and low MD human tissues implanted in the murine biochambers were taken from a high-risk population. In our study sample of 15 women, seven women were BRCA1/2 mutation carriers. Since the malignancy risk associated with MD is independent of BRCA mutation status [28,29], we expect no observable difference in the MD phenotype of the chamber tissue between the two groups. In this study, there was no difference in the stromal, adipose or glandular areas of biochamber tissues originating from women who were gene carriers and those who were not. This is supported by our previous finding that there was no difference in the MD histological phenotype of human breast core biopsies by BRCA1/2 mutation status [13].

Steroid hormones such as oestrogen and progesterone hormone replacement therapy (HRT) can increase MD directly [30,31]. The majority of the women in our study were pre-menopausal: in the sample of 15 women, only one was post-menopausal. Thus we would expect minimal effect (towards reduction in MD) due to age-related involution, or HRT usage.

Finally, in our study design, we performed selective biopsies of matched high and low MD tissue from within the same breast of each woman, then implanted these into chambers in paired right and left groins of host mice. This matched-pairs design enables comparison of the high and low MD chamber tissue without the effect of potential confounders, including the BRCA mutation status, menopausal status, and parity of the women, as well as process-related factors in the murine model.

Conclusion

Immunohistochemical staining confirms the persistence of human glandular and stromal elements in high and low MD human mammary tissue propagated within murine biochambers, while faxitron imaging demonstrates preservation of the MD differential within the model. Quantitative analyses reveal increased stromal and decreased adipose area in high compared to low MD biochamber tissues, reflecting the findings in the original mastectomy tissue [13]. Our study provides a validated platform for future studies into the biomolecular basis of MD as a risk factor for breast cancer. The correlation of the effects of modifying factors on PMD, and the changes brought about by such agents on breast tissue histology, proliferative state and stroma, is an important area for further research. Our experimental model may prove a useful tool to further elucidate the role of hormonal factors and mitogens, by assessing dynamic changes in the MD phenotype.

Competing interests

The authors declare that they have no competing interests.

Acknowledgements

This work was supported by the Victorian Breast Cancer Research Consortium (MCS, IGC, EWT, JH), the St Vincent's Hospital Research Endowment Fund (EWT, JC, PH 2008, 2009), and National Health and Medical Research Council (GLC, MCS, JH, IGC). SJL is supported by the NSS-PhD scholarship from the Agency for Science, Technology, and Research (A*STAR). St Vincent's Institute and The O'Brien Institute receive infrastructure funding from the Victorian State Government under the Medical Research Operational Infrastructure program. We thank Sue MacAuley and Nadine Wood (St Vincent's BreastScreen, St Vincent's Hospital, Victoria) for help with radiography and tissue sampling; The Victorian Cancer Biobank (Peter MacCallum Cancer Centre) for help with tissue accrual; The Department of Pathology, St Vincent's Hospital Melbourne, for assistance with tissue processing and immunohistochemical staining on the autostainer.

Figure Legends

Fig. 1 (a) and (b): H+E staining of sections in the upper panels demonstrate increased stromal and lower adipose tissue composition in high compared to low MD mastectomy tissue from within the same breast of participant 5 sampled by stereotactic biopsy. (c) and (d): H+E staining of sections in the lower panels similarly reveal increased stromal and lower adipose tissue in high compared to low MD tissue propagated in the murine biochambers from the same participant.

Fig. 2 Masson's Trichrome blue staining reveal collagen distributed circumferentially adjacent to glandular epithelium in high and low MD chamber tissue, with increased distribution of collagen in high MD chambers tissues.

Fig. 3 (a): Pan-cytokeratin staining reveals the preservation of mammary glandular structures surrounded by dense stromal tissue in a high MD chamber tissue section (participant 2). (b) Vimentin staining reveal preserved human stromal elements in a propagated high MD chamber tissue section (participant 2). (c) and (d): Human antimitochondrial antibody staining, visible as brown-stained organelles within cells of human origin in high and low MD biochamber tissue sections, demonstrate conservation of human mammary ducts and lobules,.

Fig. 4 ER staining of the glandular epithelial cells in high and low MD mastectomy sections was strongly positive, and similarly corresponds to strongly positive ER staining of epithelial cells in high and low MD biochamber tissue sections (upper panels). ER uptake was most prominent in the luminal epithelial cells (lower panels).

Fig. 5 Ki67 staining of proliferating epithelial cells in high and low MD mastectomy and biochamber tissue sections (upper panels). Ki67 uptake was greater in the glandular and stromal cells of high and low MD biochamber tissue, compared to mastectomy tissue (lower panels).

Fig. 6 (a): Scatter plot graphs of each tissue element in high and low MD biochambers demonstrate increased stromal and decreased adipose percentage areas, but no difference in glandular percentage area. (b): Scatter plot graphs of each tissue element in the parental high and low MD mastectomy biopsies similarly demonstrate increased stromal and decreased adipose percentage areas, but no difference in glandular percentage area.

Fig. 7 Scatter plot graphs of each tissue element in high MD biochambers comparing tissue originating from women with BRCA1/2 mutations and non-carriers reveal no difference in stromal, glandular or adipose percentage area.

Fig. 8 Scatter plot graph comparing the relative densitometry of high and low MD biochamber tissue after post-propagation Faxitron imaging demonstrate increased densitometry of high MD biochamber tissue.

Supplementary Figure Legends

S Fig. 1 Method for propagation of high and low MD biochamber tissue. (a): Stereotactic core biopsies of high (red circle) and low (yellow cross) MD regions are taken from the mastectomy specimen of each woman, with defects seen at sites of high and low MD tissue sampling post-biopsy. (b): A silicone biochamber is implanted around the epigastric pedicle in each groin of a SCID mouse with microsurgery techniques. The minced high and low MD material, with Matrigel and FGF-2, is transferred into the right and left biochamber respectively, and propagated for six weeks before harvest for histological and radiographic examination.

S Fig. 2 The scatter plot graph of glandular count in high and low MD groups did not demonstrate any difference in the number of glands observed.

S Fig. 3 (a) Faxitron imaging of pairs of high and low MD biochamber tissue harvested from the right and left groins, respectively, of mice (participants 4 and 5) demonstrate whiter high MD tissue on a grey background. (b) The signal intensity of the high MD biochamber tissue was greater than the low MD biochamber tissue from the same mouse.

S Fig. 4 (a) Human anti mitochondrial Ab staining did not reveal uptake in small murine glands surrounded by fat. (b) Murine-active vimentin staining of a tissue section of low MD biochamber tissue demonstrate brown nuclear staining of the adipocytes.

Tables

Table 1 Demographic characteristics of participants in the study, including their age, Birads category, family history, menopausal status, parity and past history of breast disease.

Participant	Age	Birads Category[a]	Family history	Menopausal Status	Parity	Past history of other breast disease
D1	35	2	BRCA1	Pre	2	Nil
D2	48	4	BRCA2	Pre	2	Left DCIS[c]
D3	43	2	BRCA1	Pre	2	Nil
D4	45	3	BRCA2	Pre	1	Nil
D5	59	2	Not BRCA carrier, strong FHx[b]	Post	3	Left BC[d]
P1	38	4	Not BRCA carrier, 1 second degree relative with BC	Pre	2	Left BC
P2	47	2	BRCA2	Pre	2	Nil
P3	57	2	Not BRCA carrier, no FHx	Pre	3	Left DCIS
P4	50	3	Not BRCA carrier, no FHx	Pre	2	Left DCIS
P5	41	3	Not BRCA carrier,	Pre	2	Nil

			strong FHx			
P6	41	2	Not BRCA carrier, no FHx	Pre	2	Right BC
P7	45	3	BRCA2	Pre	0	Nil
P8	50	2	Not BRCA carrier, no FHx	Pre	2	Nil
P9	43	3	BRCA2	Pre	0	Right BC
P10	44	4	Not BRCA carrier, no FHx	Pre	0	Left DCIS

a) Birads categories. 1: Predominantly fat, 2: Scattered fibroglandular densities, 3: Heterogeneously dense, 4: Extremely dense. b) FHx = Family history. c) DCIS = ductal carcinoma in situ. d) BC = breast cancer.

Table 2 Histopathology results of operative specimens from the study sample, including operation performed and histology results.

Participant	Operation performed	Histology results
D1	Bilateral skin sparing mastectomy – sample from left side	Right mastectomy: 15 mm high grade DCIS[a] of solid and cribiform type with comedo-necrosis and microcalcification, ER and PR[b] negative, weakly positive for cerbB2 (1+). No invasive malignancy. Left mastectomy: no abnormality
D2	Bilateral skin sparing mastectomy – sample from right side	Right mastectomy: MDE[c]. No in situ or invasive malignancy Left mastectomy: Old fibrous scar. No in situ or invasive malignancy

D3	Bilateral skin sparing mastectomy – sample from left side	Bilateral mastectomy: FCC[d], MDE. No evidence of malignancy
D4	Bilateral skin sparing mastectomy – sample from right side	Right mastectomy: No abnormality Left mastectomy: FCC with radial scar. No in situ or invasive malignancy.
D5	Bilateral skin sparing mastectomy – sample from right side	Right mastectomy: MDE. No in situ or invasive malignancy. Left mastectomy: Old fibrous scar. No in situ or invasive malignancy.
P1	Left skin sparing mastectomy - sample from left side	Left mastectomy: 6 mm DCIS with microcalcification, FCC
P2	Left skin sparing mastectomy - sample from left side	Left mastectomy: FCC with fibrosis and adenosis
P3	Right skin sparing mastectomy - sample from right side	Right mastectomy: FCC, apocrine metaplasia
P4	Left skin sparing mastectomy - sample from left side	Left mastectomy: 65 mm high grade DCIS with comedo necrosis, FCC, apocrine metaplasia
P5	Bilateral skin sparing mastectomy - sample from left side	Left and right mastectomy: FCC
P6	Left skin sparing mastectomy - sample from left side	Left mastectomy: FCC
P7	Bilateral skin sparing mastectomy - sample	Left mastectomy: 8 mm IDC[e], adjacent DCIS, ER 90%, PR 90%, Her2 negative. SN[f] negative.

	from right side	Right mastectomy: No in situ or invasive malignancy
P8	Right skin sparing mastectomy - sample from right side	Right mastectomy: 35 mm DCIS, 3 mm IDC, ER>90%, PR 1%, Her2 negative. SN negative
P9	Bilateral skin sparing mastectomy - sample from left side	Left and right mastectomy: ALH[g], sclerosing adenosis
P10	Left skin sparing mastectomy - sample from left side	Left mastectomy: 20 mm DCIS with necrosis and microcalcification

a) DCIS = ductal carcinoma in situ. b) PR = progesterone receptor. c) MDE = mammary duct ectasia. d) FCC = fibrocystic change. e) IDC = invasive ductal carcinoma. f) SN = sentinel node. g) ALH = atypical lobular hyperplasia.

References

1. Boyd NF, Guo H, Martin LJ, Sun L, Stone J, Fishell E, Jong RA, Hislop G, Chiarelli A, Minkin S, Yaffe MJ (2007) Mammographic density and the risk and detection of breast cancer. N Engl J Med 356 (3):227-236. doi:356/3/227 [pii]
10.1056/NEJMoa062790

2. Boyd NF, Rommens JM, Vogt K, Lee V, Hopper JL, Yaffe MJ, Paterson AD (2005) Mammographic breast density as an intermediate phenotype for breast cancer. Lancet Oncol 6 (10):798-808. doi:S1470-2045(05)70390-9 [pii]
10.1016/S1470-2045(05)70390-9

3. McCormack VA, dos Santos Silva I (2006) Breast density and parenchymal patterns as markers of breast cancer risk: a meta-analysis. Cancer Epidemiol Biomarkers Prev 15 (6):1159-1169. doi:15/6/1159 [pii]
10.1158/1055-9965.EPI-06-0034

4. Ursin G, Ma H, Wu AH, Bernstein L, Salane M, Parisky YR, Astrahan M, Siozon CC, Pike MC (2003) Mammographic density and breast cancer in three ethnic groups. Cancer Epidemiol Biomarkers Prev 12 (4):332-338

5. Byrne C, Schairer C, Wolfe J, Parekh N, Salane M, Brinton LA, Hoover R, Haile R (1995) Mammographic features and breast cancer risk: effects with time, age, and menopause status. J Natl Cancer Inst 87 (21):1622-1629

6. Boyd NF, Byng JW, Jong RA, Fishell EK, Little LE, Miller AB, Lockwood GA, Tritchler DL, Yaffe MJ (1995) Quantitative classification of mammographic densities and breast cancer risk: results from the Canadian National Breast Screening Study. J Natl Cancer Inst 87 (9):670-675

7. Wolfe JN, Saftlas AF, Salane M (1987) Mammographic parenchymal patterns and quantitative evaluation of mammographic densities: a case-control study. AJR Am J Roentgenol 148 (6):1087-1092

8. Byrne C, Schairer C, Brinton LA, Wolfe J, Parekh N, Salane M, Carter C, Hoover R (2001) Effects of mammographic density and benign breast disease on breast cancer risk (United States). Cancer Causes Control 12 (2):103-110

9. Cuzick J, Warwick J, Pinney E, Duffy SW, Cawthorn S, Howell A, Forbes JF, Warren RM (2011) Tamoxifen-induced reduction in mammographic density and breast cancer risk reduction: a nested case-control study. J Natl Cancer Inst 103 (9):744-752. doi:djr079 [pii]
10.1093/jnci/djr079
10. Boyd NF (2011) Tamoxifen, mammographic density, and breast cancer prevention. J Natl Cancer Inst 103 (9):704-705. doi:djr115 [pii]
10.1093/jnci/djr115
11. Guo YP, Martin LJ, Hanna W, Banerjee D, Miller N, Fishell E, Khokha R, Boyd NF (2001) Growth factors and stromal matrix proteins associated with mammographic densities. Cancer Epidemiol Biomarkers Prev 10 (3):243-248
12. Warren R (2004) Hormones and mammographic breast density. Maturitas 49 (1):67-78. doi:10.1016/j.maturitas.2004.06.013
S0378-5122(04)00212-9 [pii]
13. Lin SJ, Cawson J, Hill P, Haviv I, Jenkins M, Hopper JL, Southey MC, Campbell IG, Thompson EW (2011) Image-guided sampling reveals increased stroma and lower glandular complexity in mammographically dense breast tissue. Breast Cancer Res Treat 128 (2):505-516. doi:10.1007/s10549-011-1346-0
14. Hariri M, Wood GA, DiGrappa MA, MacPherson M, Backman SA, Yaffe MJ, Mak TW, Boyd NF, Khokha R (2004) Experimental manipulation of radiographic density in mouse mammary gland. Breast Cancer Res 6 (5):R540-545. doi:10.1186/bcr901
bcr901 [pii]
15. Kelly JL, Findlay MW, Knight KR, Penington A, Thompson EW, Messina A, Morrison WA (2006) Contact with existing adipose tissue is inductive for adipogenesis in matrigel. Tissue Eng 12 (7):2041-2047. doi:10.1089/ten.2006.12.2041
16. Stillaert F, Findlay M, Palmer J, Idrizi R, Cheang S, Messina A, Abberton K, Morrison W, Thompson EW (2007) Host rather than graft origin of Matrigel-induced adipose tissue in the murine tissue-engineering chamber. Tissue Eng 13 (9):2291-2300. doi:10.1089/ten.2006.0382
17. Li T, Sun L, Miller N, Nicklee T, Woo J, Hulse-Smith L, Tsao MS, Khokha R, Martin L, Boyd N (2005) The association of measured breast tissue characteristics with mammographic density and other risk factors for breast cancer. Cancer Epidemiol Biomarkers Prev 14 (2):343-349. doi:14/2/343 [pii]

10.1158/1055-9965.EPI-04-0490

18. Ursin G, Hovanessian-Larsen L, Parisky YR, Pike MC, Wu AH (2005) Greatly increased occurrence of breast cancers in areas of mammographically dense tissue. Breast Cancer Res 7 (5):R605-608. doi:bcr1260 [pii]

10.1186/bcr1260

19. Gill JK, Maskarinec G, Pagano I, Kolonel LN (2006) The association of mammographic density with ductal carcinoma in situ of the breast: the Multiethnic Cohort. Breast Cancer Res 8 (3):R30. doi:bcr1507 [pii]

10.1186/bcr1507

20. Provenzano PP, Inman DR, Eliceiri KW, Keely PJ (2009) Matrix density-induced mechanoregulation of breast cell phenotype, signaling and gene expression through a FAK-ERK linkage. Oncogene 28 (49):4326-4343. doi:onc2009299 [pii]

10.1038/onc.2009.299

21. Wang JG, Miyazu M, Xiang P, Li SN, Sokabe M, Naruse K (2005) Stretch-induced cell proliferation is mediated by FAK-MAPK pathway. Life Sci 76 (24):2817-2825. doi:S0024-3205(05)00072-X [pii]

10.1016/j.lfs.2004.10.050

22. Tlsty TD, Coussens LM (2006) Tumor stroma and regulation of cancer development. Annu Rev Pathol 1:119-150. doi:10.1146/annurev.pathol.1.110304.100224

23. Shackleton M, Vaillant F, Simpson KJ, Stingl J, Smyth GK, Asselin-Labat ML, Wu L, Lindeman GJ, Visvader JE (2006) Generation of a functional mammary gland from a single stem cell. Nature 439 (7072):84-88. doi:nature04372 [pii]

10.1038/nature04372

24. Ghosh K, Brandt KR, Reynolds C, Scott CG, Pankratz VS, Riehle DL, Lingle WL, Odogwu T, Radisky DC, Visscher DW, Ingle JN, Hartmann LC, Vachon CM (2011) Tissue composition of mammographically dense and non-dense breast tissue. Breast Cancer Res Treat. doi:10.1007/s10549-011-1727-4

25. Lyons TR, O'Brien J, Borges VF, Conklin MW, Keely PJ, Eliceiri KW, Marusyk A, Tan AC, Schedin P (2011) Postpartum mammary gland involution drives progression of ductal carcinoma in situ through collagen and COX-2. Nat Med 17 (9):1109-1115. doi:nm.2416 [pii]

10.1038/nm.2416

26. Levental KR, Yu H, Kass L, Lakins JN, Egeblad M, Erler JT, Fong SF, Csiszar K, Giaccia A, Weninger W, Yamauchi M, Gasser DL, Weaver VM (2009) Matrix crosslinking forces tumor progression by enhancing integrin signaling. Cell 139 (5):891-906. doi:S0092-8674(09)01353-1 [pii] 10.1016/j.cell.2009.10.027

27. McGinley JN, Thompson HJ (2011) Quantitative assessment of mammary gland density in rodents using digital image analysis. Biol Proced Online 13 (1):4. doi:1480-9222-13-4 [pii] 10.1186/1480-9222-13-4

28. Gierach GL, Loud JT, Chow CK, Prindiville SA, Eng-Wong J, Soballe PW, Giambartolomei C, Mai PL, Galbo CE, Nichols K, Calzone KA, Vachon C, Gail MH, Greene MH (2010) Mammographic density does not differ between unaffected BRCA1/2 mutation carriers and women at low-to-average risk of breast cancer. Breast Cancer Res Treat 123 (1):245-255. doi:10.1007/s10549-010-0749-7

29. Mitchell G, Antoniou AC, Warren R, Peock S, Brown J, Davies R, Mattison J, Cook M, Warsi I, Evans DG, Eccles D, Douglas F, Paterson J, Hodgson S, Izatt L, Cole T, Burgess L, Eeles R, Easton DF (2006) Mammographic density and breast cancer risk in BRCA1 and BRCA2 mutation carriers. Cancer Res 66 (3):1866-1872. doi:66/3/1866 [pii] 10.1158/0008-5472.CAN-05-3368

30. Greendale GA, Reboussin BA, Slone S, Wasilauskas C, Pike MC, Ursin G (2003) Postmenopausal hormone therapy and change in mammographic density. J Natl Cancer Inst 95 (1):30-37

31. Rutter CM, Mandelson MT, Laya MB, Seger DJ, Taplin S (2001) Changes in breast density associated with initiation, discontinuation, and continuing use of hormone replacement therapy. JAMA 285 (2):171-176. doi:joc01079 [pii]

Figure
Click here to download Figure: Figures MD model 8.pptx

Fig. 1

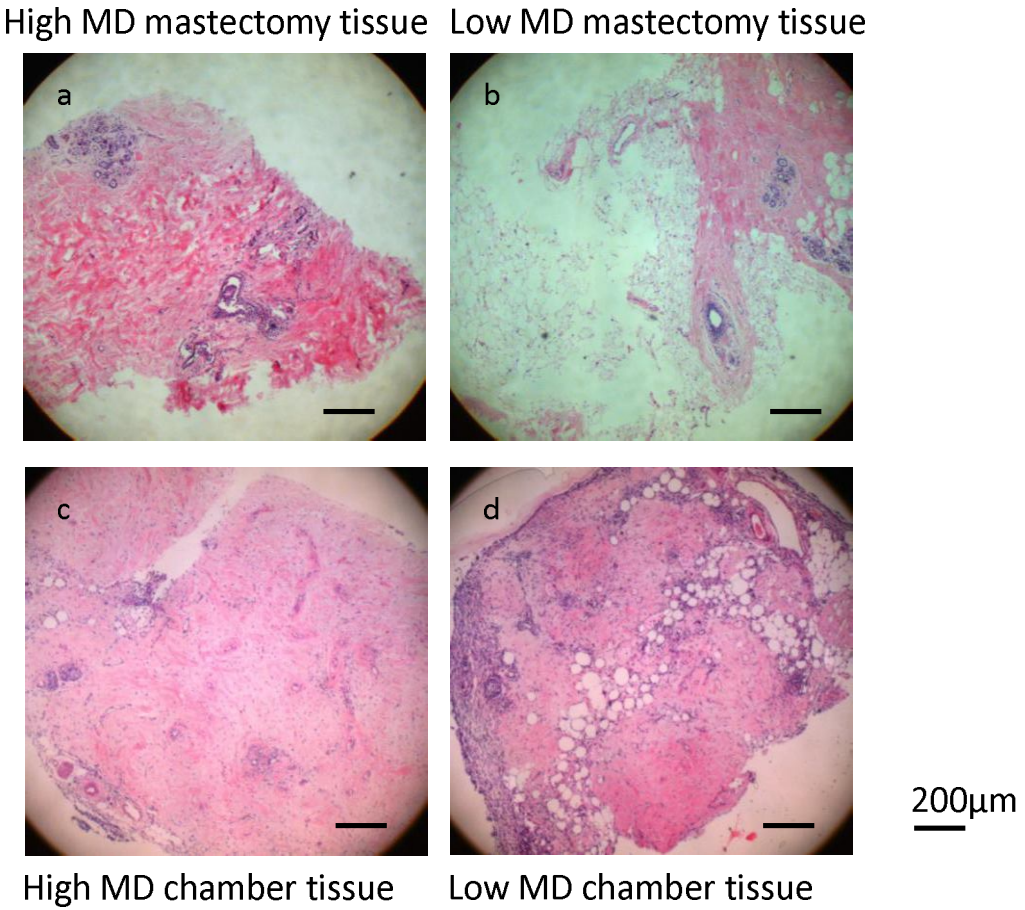

Fig. 2

High MD chamber tissue

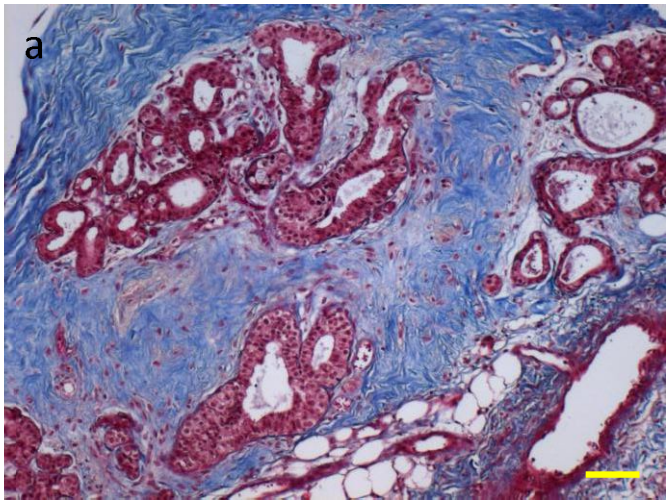

Low MD chamber tissue

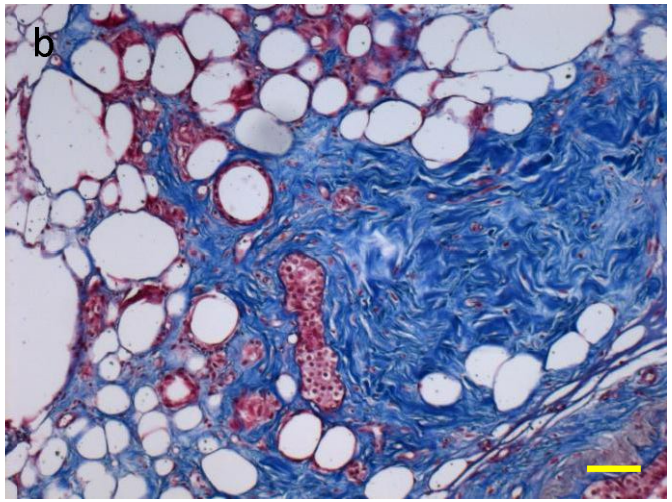

100µm

Fig. 3

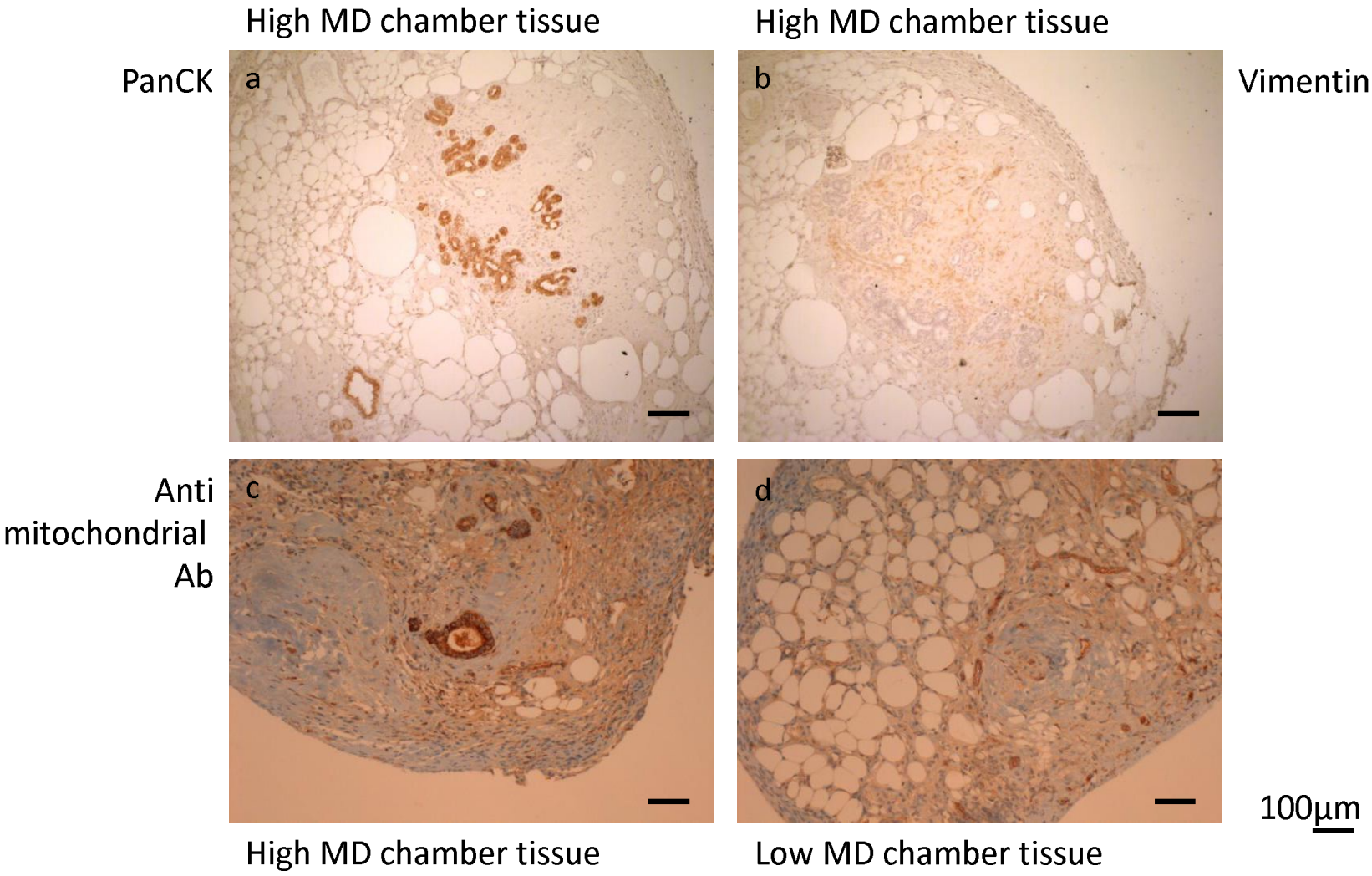
High MD chamber tissue
High MD chamber tissue
PanCK
a
b
Vimentin
Anti mitochondrial Ab
c
d
100µm
High MD chamber tissue
Low MD chamber tissue

Fig. 4

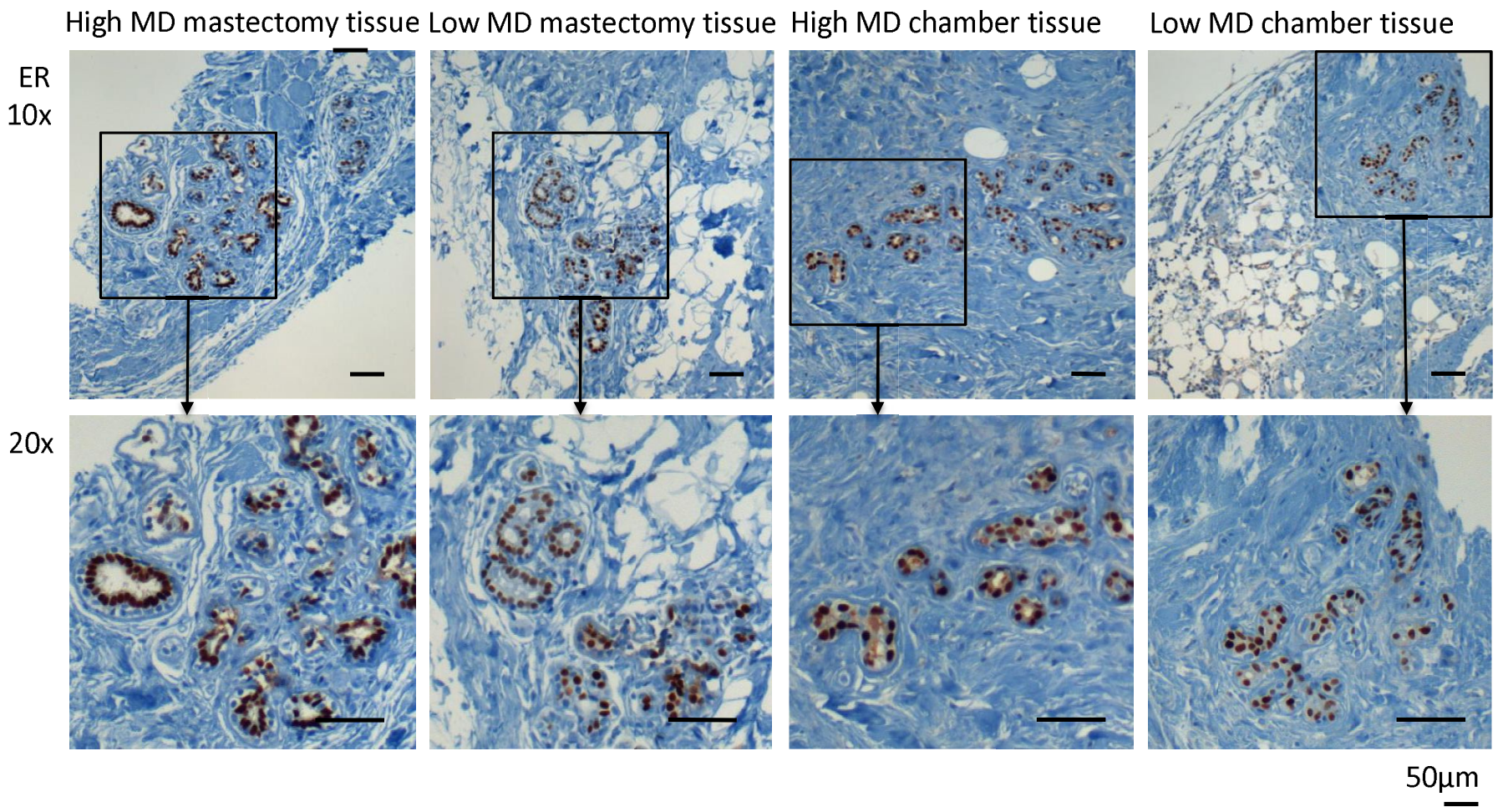
High MD mastectomy tissue
Low MD mastectomy tissue
High MD chamber tissue
Low MD chamber tissue
ER
10x
20x
50µm

Fig. 5

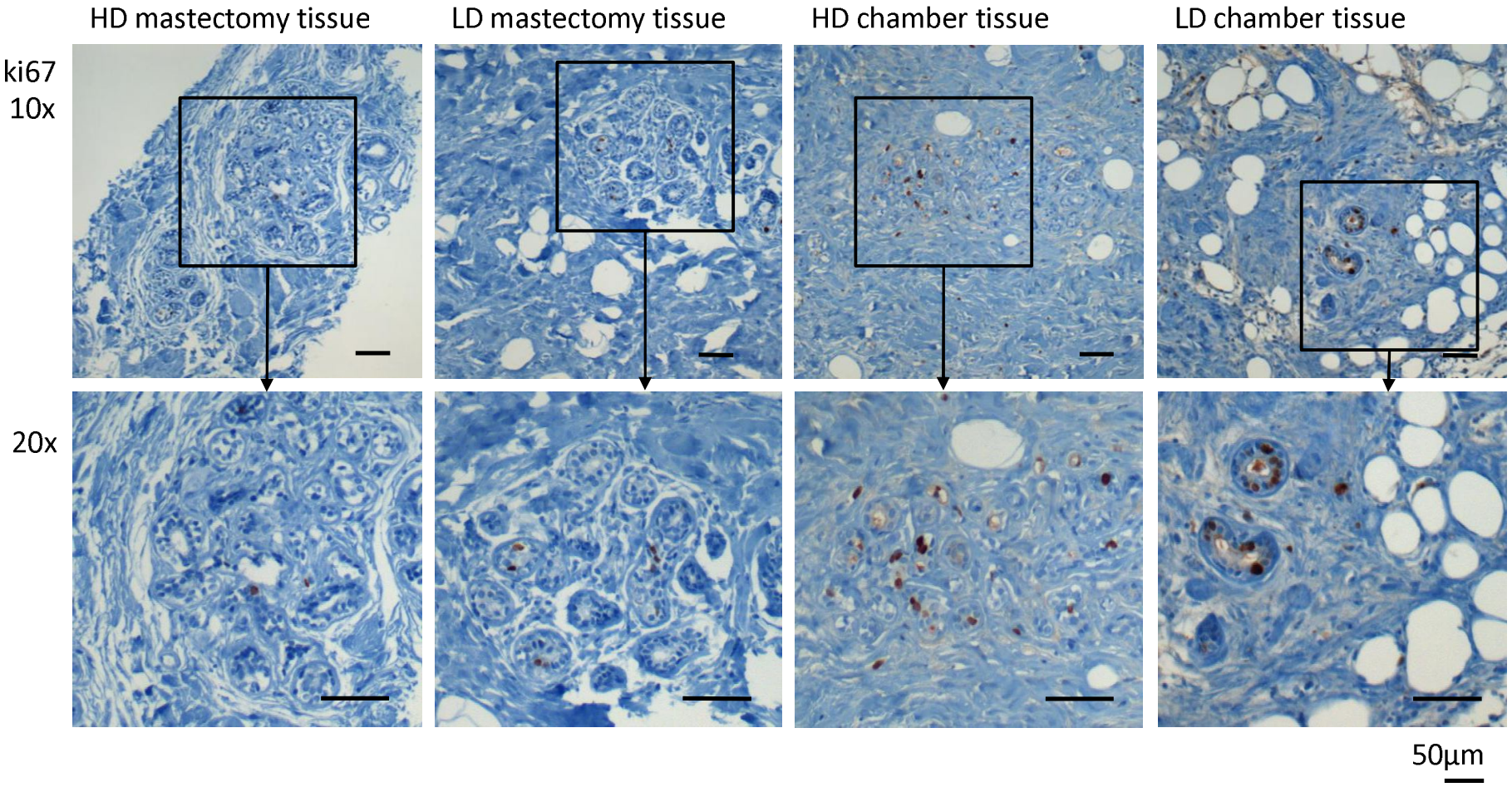
HD mastectomy tissue
LD mastectomy tissue
HD chamber tissue
LD chamber tissue
ki67
10x
20x
50µm

Fig. 6

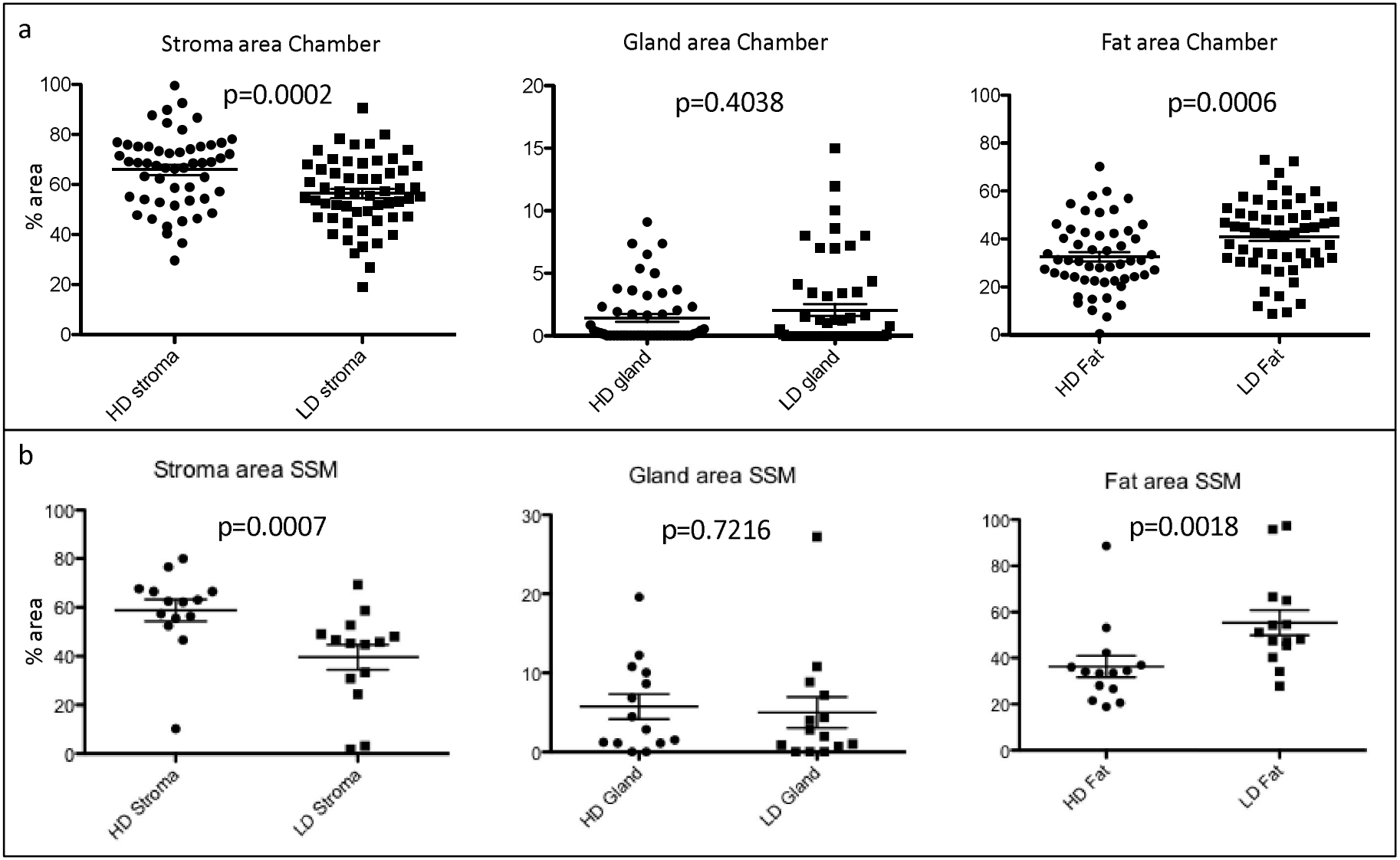
a
Stroma area Chamber
p=0.0002
% area
HD stroma
LD stroma
Gland area Chamber
p=0.4038
HD gland
LD gland
Fat area Chamber
p=0.0006
HD Fat
LD Fat
b
Stroma area SSM
p=0.0007
% area
HD Stroma
LD Stroma
Gland area SSM
p=0.7216
HD Gland
LD Gland
Fat area SSM
p=0.0018
HD Fat
LD Fat

Fig. 7

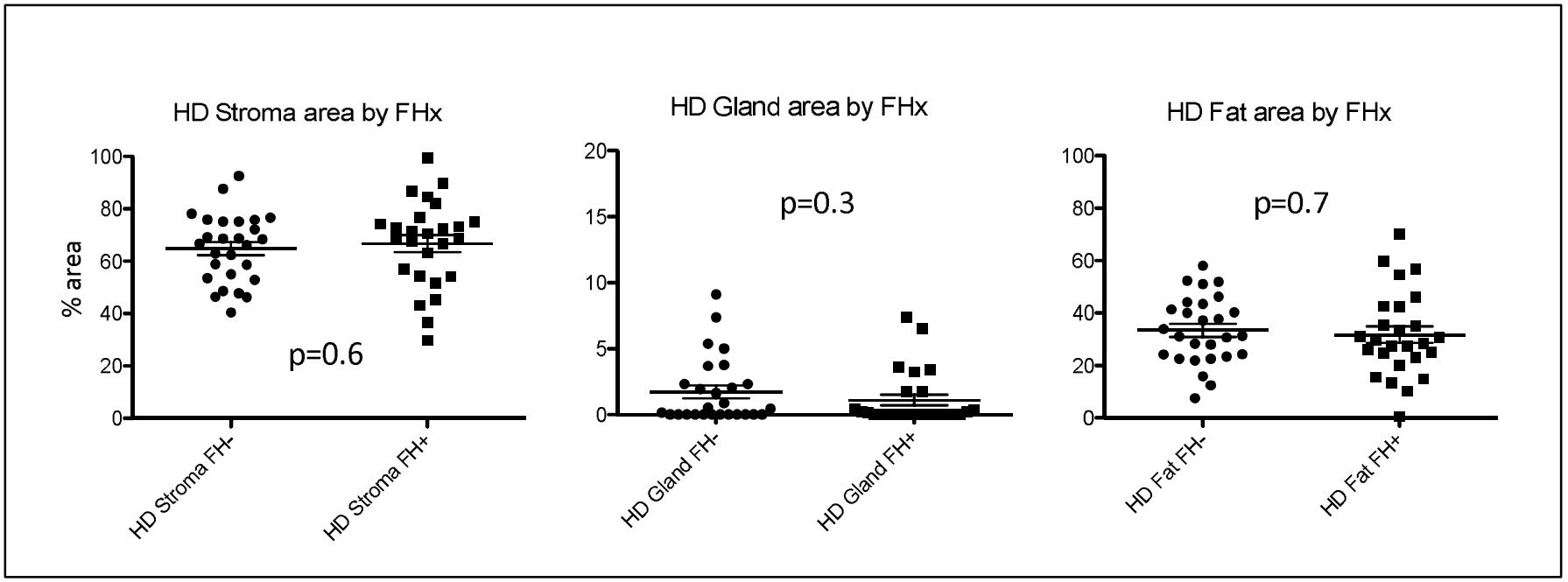
HD Stroma area by FHx
% area
100
80
60
40
20
0
p=0.6
HD Stroma FH-
HD Stroma FH+
HD Gland area by FHx
20
15
10
5
0
p=0.3
HD Gland FH-
HD Gland FH+
HD Fat area by FHx
100
80
60
40
20
0
p=0.7
HD Fat FH-
HD Fat FH+

Fig. 8

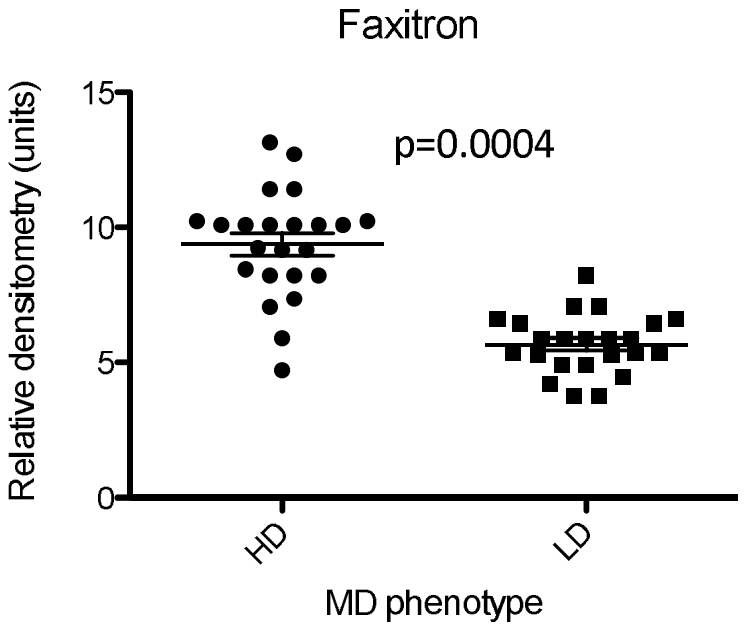
Faxitron
Relative densitometry (units)
15
10
5
0
p=0.0004
HD
LD
MD phenotype